A search for 22-GHz water masers within the giant molecular cloud associated with RCW 106

Author:
Breen, S. L.; Ellingsen, S. P.; Johnston-Hollitt, M.; Wotherspoon, S.; Bains, Indra; Burton, Michael; Cunningham, M.; Lo, N; Senkbeil, C. E.; Wong, T.

A search for 22-GHz water masers within the giant molecular cloud associated with RCW 106

A search for 22-GHz water masers within the giant molecular cloud associated with RCW 106

S. L. Breen,[1] S. P. Ellingsen,[1] M. Johnston-Hollitt,[1] S. Wotherspoon,[1] I. Bains,[2,3]
M. G. Burton,[2] M. Cunningham,[2] N. Lo,[2] C. E. Senkbeil[1] and T. Wong[2,4]

[1] *School of Mathematics and Physics, University of Tasmania, Private Bag 21, Hobart, Tasmania 7001, Australia;*
Shari.Breen@utas.edu.au
[2] *School of Physics, University of New South Wales, Sydney, NSW 2052, Australia*
[3] *Centre for Astrophysics and Supercomputing, Swinburne University of Technology, P.O. Box 218, Hawthorn, VIC 3122, Australia*
[4] *Australia Telescope National Facility, CSIRO, PO Box 76, Epping, NSW 1710, Australia*

30 October 2006

ABSTRACT

We report the results of a blind search for 22-GHz water masers in two regions, covering approximately half a square degree, within the giant molecular cloud associated with RCW 106. The complete search of the two regions was carried out with the 26-m Mount Pleasant radio telescope and resulted in the detection of nine water masers, five of which are new detections. Australia Telescope Compact Array (ATCA) observations of these detections have allowed us to obtain arcsecond accurate positions, allowing meaningful comparison with infrared and molecular data of the region. We find that for the regions surveyed there are more water masers than either 6.7-GHz methanol, or main-line OH masers. The water masers are concentrated towards the central axis of the star formation region, in contrast to the 6.7-GHz methanol masers which tend to be located near the periphery. The colours of the GLIMPSE point sources associated with the water masers are similar to those for 6.7-GHz methanol masers, but perhaps less red. We have made statistical investigation of the properties of the ^{13}CO and 1.2-mm dust clumps with and without associated water masers. We find that the water masers are associated with the more massive, denser and brighter ^{13}CO and 1.2-mm dust clumps. We present statistical models that are able to predict with low misclassification rate, those ^{13}CO and 1.2-mm dust clumps that are likely to have associated water masers.

Key words: masers - ISM: molecules - radio lines: general - stars: formation.

1 INTRODUCTION

From soon after the first detection of 22-GHz water maser emission in the sources Sgr B2, Orion and W 49 in 1969 (Cheung et al. 1969) they have been regarded as one of the best indicators of star formation. The 22-GHz $6_{1,6} \rightarrow 5_{2,3}$ rotational transition of H_2O is the brightest spectral line at radio wavelengths and traces shocked gas in star formation regions, outflows, as well as dense circumstellar shells around evolved stars. Emission from this transition often exhibits significantly greater temporal variability than is commonly observed in other interstellar maser species such as OH and methanol (Brand et al. 2003). The physical conditions required to produce water maser excitation are high densities (10^7-10^9 cm^{-3}) and temperatures of a few 100 K (Elitzur, Hollenbach & McKee 1989), both of which are seen in the in-

ner parts of circumstellar disks around young stellar objects and in regions of shocked gas (Torrelles et al. 2002).

Interstellar masers from water (e.g. Valdettaro et al. 2001), OH (e.g. Caswell 1998) and methanol (e.g. Pestalozzi, Minier & Booth 2005) transitions have been detected towards hundreds of star formation regions in our Galaxy, with many of these showing emission from more than one species. While there have been a number of large-scale untargeted searches for OH (Caswell, Haynes & Goss 1980) and methanol (Ellingsen et al. 1996; Szymczak et al. 2002), previous searches for water masers in star formation regions have typically targeted ultracompact HII regions selected on the basis of *IRAS* (Infrared Astronomy Satellite) colours (e.g. Churchwell, Walmsley & Cesaroni 1990), or other sources believed to be high-mass young stellar objects (e.g. Beuther, Walsh & Schilke 2002). To date there have been no large

2   *S. L. Breen et al.*

untargeted surveys for water masers primarily because at a frequency of 22 GHz telescope beam sizes are approximately one-third the size of those at 6.7-GHz, the frequency of the strongest methanol maser transition, and hence require approximately an order of magnitude more pointings. Here we present an untargeted search for water masers within the giant molecular cloud (GMC) complex associated with RCW 106. The GMC is located at a distance of 3.6 kpc (Lockman 1979) and was discovered by Gillespie et al. (1977) during observations of molecular clouds associated with southern Galactic HII regions in the J=1-0 transition of CO. These observations uncovered a number of bright HII regions along a line which is almost parallel to the Galactic plane including one of the brightest infrared sources in our Galaxy, *IRAS*16183-4958 (Becklin et al. 1973), which is associated with the HII region G 333.6-0.2.

The GMC is roughly centred on $l \sim 333°$, $b \sim -0°.5$ (or α_{j2000}=16:21, δ_{j2000}=-50:20) and extends approximately $1°.2 \times 0°.6$ on the sky (or approximately 90 pc x 30 pc at an assumed distance of 3.6 kpc) (Bains et al. 2006). This region passes through the ring of molecular clouds that circle the Galaxy at around 5 kpc from its centre (e.g. Simon et al. 2001) and exhibits a diverse range of molecular regions, bright HII regions, GLIMPSE (*Spitzer* Galactic Legacy Infrared Mid-Plane Survey Extraordinaire) point sources, *IRAS* and *MSX* (Midcourse Space Experiment) sources all of which are embedded in a larger region of diffuse atomic and molecular gas.

Observations of the ^{13}CO J=1-0 transition at 110 GHz by Bains et al. (2006) showed the velocity structure of the region to contain five primary velocity components, with the dominent feature centred on $v_{LSR} \sim$ -50 km s^{-1}. Analysis of the integrated ^{13}CO data using the *CLUMPFIND* algorithm of Williams, de Geus & Blitz (1994) identified 61 ^{13}CO clumps. The ^{13}CO emission takes the form of a string of knots with the clumps arranged along an axis aligned NW to SE (Bains et al. 2006).

This GMC has been the focus of numerous observations in recent times, including far-infrared (FIR) observations of the dust continuum at 150 and 210 μm which identified 23 emission peaks with dust temperatures between 20 and 40 K (Karnik et al. 2001). The region was also observed by Mookerjea et al. (2004) using SIMBA (SEST IMaging Bolometer Array) on Swedish European Southern Observatory Submillimetre Telescope (SEST) who obtained a 1.2-mm dust continuum image of the region. Mookerjea et al. (2004) identified 95 dust emission peaks (or clumps), half of which have *MSX* counterparts. Observations of a multitude of molecular lines towards detected HII regions and *IRAS* sources indicate probable ongoing star formation (Mookerjea et al. 2004). These observations, like those of Bains et al. (2006) have identified that the GMC has a linear clumpy structure.

Complete surveys of the GMC region have been carried out by Ellingsen et al. (1996) for 6.7-GHz methanol masers and Caswell, Haynes & Goss (1980) for 1665- and 1667-MHz OH masers. These surveys resulted in the detection of nine methanol and six OH masers within the region surveyed in ^{13}CO by Bains et al. (2006). Five water masers have also been detected within this region in targeted searches made by Johnston et al. (1972), Caswell et al. (1974), Batchelor et al. (1980) and Braz & Scalise (1982).

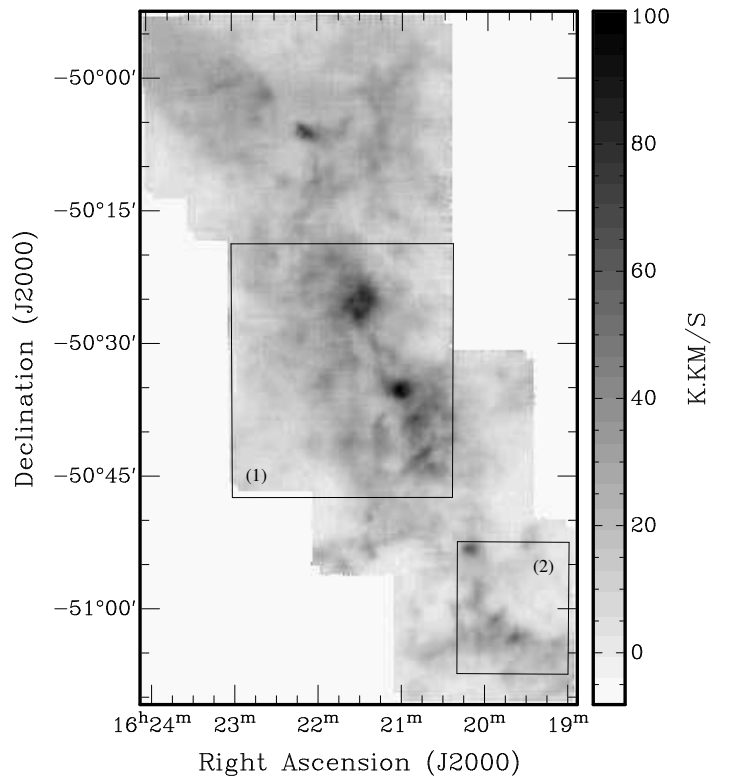Here, we present the results of an untargeted survey

Figure 1. Integrated ^{13}CO emission observed by Bains et al. (2006) with the two regions surveyed for water masers overlaid.

made with the University of Tasmania Mount Pleasant 26-m radio telescope for 22-GHz water masers. The survey covers two distinct regions within the GMC. The first (hereafter Region 1) is a $0°.50 \times 0°.42$ area centered on $l \sim 333$, $b \sim -0°.5$. This region encompasses much of the high density gas and dust regions identified by Karnik et al. (2001), Mookerjea et al. (2004) and Bains et al. (2006) in the central section of the GMC. Region 1 also contains one previously detected 22-GHz water maser, G 333.13-0.43, discovered by Caswell et al. (1974). The second region (hereafter, Region 2) covers a $0°.28 \times 0°.24$ area of the GMC and is approximately centred on well-known optically visible HII region RCW 106. This region contains two previously detected water masers. The extent of the two regions compared to the integrated ^{13}CO emission are shown in Figure 1.

The GMC is the focus of an ongoing project to characterise the turbulence in the molecular cloud and compare this to the star formation efficiency in order to attain a relationship between the two. Commencing in 2004 a multitude of millimetre molecular line transitions (including ^{13}CO (Bains et al. 2006), CS, C$_{34}$S, C$_{18}$O, C$_2$H, HCN, H$_{13}$CN, HCO$^+$, H$_{13}$CO$^+$, HNC, CH$_3$OH and SiO) have been observed by the Delta quadrant survey team at the University of New South Wales[1]. Interstellar masers require special physical conditions and the different specices are generally thought to trace a particular evolutionary phases of the

---

[1] http://www.phys.unsw.edu.au/astro/mopra/dqs.php

high-mass star formation process. Through combining information on all the strong and common interstellar maser transitions with millimeter molecular line and other existing infrared and millimeter continuum data we aim to better understand the evolutionary phases traced by each type of maser.

2   OBSERVATIONS & DATA PROCESSING

The primary search for 22-GHz water masers towards the G 333.2-0.6 GMC was undertaken between 2005 April-November using the University of Tasmania's 26-m radio telescope at Mount Pleasant. The observations were made with a cryogenically cooled receiver that detects both left and right circularly polarized signals and has a typical system equivalent flux density of 2000-2200 Jy in good weather at elevations above about 40 degrees. At 22 GHz the telescope has a 2.2 arcminute half power beam width (HPBW) and at the time of the observations the measured RMS pointing errors were ∼1 arcminute. The data were recorded using a 2-bit auto-correlation spectrometer configured with 2048 spectral channels per polarisation over a 32 MHz bandwidth, which was centred on an LSR velocity of approximately -40 km s^{-1}. The observations covered a velocity range of 430 km s^{-1} with a spectral resolution of 0.25 km s^{-1}. The two regions were surveyed using an equilateral triangle pattern with each pointing separated by 1.1 arcminutes (half of the HPBW) from all adjacent grid points. Each pointing was observed for a total onsource integration time of nine minutes and the typical noise level in each spectrum was 1 Jy (see below for further details). The water maser G 333.608-0.215, discovered by Johnston et al. (1972), was observed at the beginning of each observing session to test the system and ensure consistency. Although it is not located in either of the survey regions we have included it in the nine masers detected in this survey.

The weather conditions in which the observations were made varied substantially, and in general the conditions under which data were taken in Region 1 was of a much more favourable standard. In order to minimise atmospheric and telescope pointing effects all observations were made above an elevation of 40 degrees. Data affected by poor weather conditions were reobserved (in some cases on multiple occasions), however a small percentage of the data has significantly poorer sensitivity limit than the rest. The observations of Region 1 required approximately 750 pointings while Region 2 was much smaller containing just under 300 pointings. The majority (78 percent) of the data taken in region 1 had an RMS noise level of less than 1 Jy while the remaining (22 percent of) data in this region was subject to an RMS noise level of between 1 Jy and 2 Jy after box car smoothing over 5 channels and averaging the two polarisations together. This equates to a 5σ detection limit of 5 Jy over the majority of the region, with a maximum of 10 Jy in the worst affected pointings. In region 2 only 35 percent of pointings has an RMS noise level of less than 1 Jy and the remaining 65 percent had an RMS noise of up to 5 Jy. This equates to a 5σ detection limit between 5 and 25 Jy, hence our ability to detect weaker masers within region 2 is greatly reduced.

For each detected water maser additional observations

consisting of a 5-point grid (centred on the preliminary position) were made to better determine the location of the emission. The position was determined by fitting a 2D circular Gaussian (with the same HPBW as the telescope) to the relative amplitudes of the strong emission in the maser spectra observed in the 5-point grid. Positions determined in this manner are accurate to approximately 1 arcminute, which is insufficient to allow meaningful comparison with millimeter and infrared observations of the region. In order to obtain accurate positions for the detected water masers we were granted two sessions of Australia Telescope Compact Array (ATCA) director's time. Preliminary observations of the masers detected in the Mount Pleasant survey were made on 2006 June 19 with the ATCA in the 1.5D configuration. The observations were centred on a frequency of 22.238 GHz with the correlator configured to record 256 spectral channels across a 16 MHz bandwidth. These observations failed to detect one of the water masers discovered in the Mount Pleasant survey (G 333.29-0.38), most likely due to temporal variability.

Further observations were made with the ATCA in the 6A configuration on 2006 July 16 & 17. In this array configuration the minimum baseline length is 337 m and the maximum is 5939 m. The observations were centred on 22.236 GHz and the correlator sampled two orthogonal linear polarisations, each processed to give a 512 channel spectrum across an 8 MHz bandwidth. Each of the maser sites detected in the earlier ATCA observations (8 in total) were observed in a series of three minute cuts over a range of hour-angles. Observations of one of the phase calibrators PKS B1613-586 and PKS B1646-50 where made for a duration of 90 seconds before and after every two maser observations (i.e. every 6 minutes). PKS B1934-638 was used as the primary flux calibrator and at 22.236 GHz has an assumed flux density of 0.83 Jy. PKS B1253-055 was used for bandpass calibration. These ATCA observations were made using reference pointing, and as arcsecond accurate positions were obtained in the initial ATCA observations all of the maser sites were close to the centre of the primary beam. Over the two days each source was observed a total of eight times, equivalent to a total on-source integration time of 24 minutes.

The data were processed using the `miriad` software package (Sault, Teuben & Wright 1995) applying the standard techniques for ATCA spectral line and continuum observations. The frequency resolution, after Hanning smoothing, was 0.038 MHz or 0.50 km s^{-1}. The RMS noise in a single spectral channel in the final data cubes was approximately 0.15 Jy and the signal-to-noise ratio of the final spectra of about 20:1 in the worst case. The RMS noise level in the continuum figures was typically around 0.02 Jy/beam. These observations have enabled us to determine the positions of the water masers to an accuracy of approximately 0.5 arcseconds.

3   RESULTS

A search of two regions near the G 333.2-0.6 giant molecular cloud resulted in the detection of nine 22-GHz water masers, five of which are new detections (Table 1), as well four 22-GHz continuum sources (see Section 3.2). Figure 2 shows the positions of all the detected water masers overlaying the

4   *S. L. Breen et al.*

integrated ^{13}CO emission observed by Bains et al. (2006), while Figure 3 shows the maser locations on a three colour GLIMPSE image of the GMC. To our knowledge, this is the first high-mass star formation complex for which untargeted searches have been made in all of main-line OH, 6.7-GHz methanol and 22-GHz water masers. Previous targeted searches for water masers towards known 6.7-GHz methanol masers achieved detection rates of around 50 percent (Szymczak, Pillai & Menten 2005). In contrast we find that only 25 percent of the 6.7-GHz methanol masers that fall within our survey region have an an associated water maser. We additionally find that only 11 percent of the water masers that we detect have an associated methanol maser which implies that targeted water maser searches towards 6.7-GHz methanol masers may not the most efficient way to increase the number of known water masers. It also supports the hypothesis that water masers may be the most prevelant species within star formation regions as our relatively insensitive survey has detected twice as many water masers as either 6.7-GHz methanol or OH in the corresponding regions.

Comparison of the water maser locations with the other maser species, the integrated ^{13}CO emission and the three colour GLIMPSE image shows that in general the water masers originate very close to the higher density molecular gas and warm dust, near the main axis of star formation within the molecular cloud. In contrast the methanol masers tend to be offset from it, close to the interface between the intense mid-infrared emission and the larger molecular cloud (Ellingsen 2006).

Spectra of the detected water masers are shown in Figures 4 and 5. The spectra have been produced by integrating the emission in the ATCA image cubes for each source. The only exception is water maser G 333.29-0.38 for which the Mount Pleasant spectrum is shown. The positional accuracy of sources detected in the ATCA observations is approximately 0.5 arcseconds and we have used three significant figures after the decimal place in their Galactic coordinate names. For the sources only detected in the Mount Pleasant component of the survey we are only justified in using 2 significant figures and have done so throughout the paper. Comments on each maser can be found in section 3.1. The newly detected water masers (Fig. 4), with one exception have a peak flux density less than 50 Jy, while the previously detected sources (Fig. 5), again with one exception, have peak flux densities greater than 100 Jy.

The 6.7-GHz methanol masers sites in this region have previously been searched for associated 22-GHz water maser emission by Hanslow (1997) who detected emission towards a number of sources (G 332.942-0.686, G 333.121-0.434, G 333.128-0.440, G 333.130-0.560, G 333.234-0.062 and G 333.466-0.164) in the G 333.2-0.6 giant molecular cloud. Three of these (G 332.942-0.686, G 333.234-0.062 and G 333.466-0.164) lie outside the regions of our untargeted search. While of the other three, only G 333.121-0.434 was detected in the current work. It appears that the emission attributed to G 333.128-0.440 by Hanslow (1997) is in fact associated with G 333.121-0.434, while that associated with G 333.130-0.560 was not detectable at the epoch of our search. Because of the uncertainty in the position of the water masers detected by Hanslow (1997) and the possibility that some may result from an unassociated strong source de-

tected in a sidelobe, in Figures 2 & 3 we have only marked those water masers detected in our current survey.

In addition to the nine water masers that we present, we made a one-time detection with the 26-m Mount Pleasant radio telescope of a water maser right on the edge of the field of observations with coordinates G 333.22-0.20. Subsequent observations showed no detectable emission and as a result we do not include it in the list of water masers that we detect. This emission consisted of a single velocity feature at -87 km s^{-1} of around 6 Jy. We believe that this emission was actually a detection of the strong water maser G 333.234-0.062 detected by Hanslow (1997). Hanslow (1997) reported G 333.234-0.062 to consists of multiple velocity features with the most prominent observed at -86 km s^{-1}, with a flux density of 108 Jy.

The majority of the water masers we detected have exhibited variability of up to a factor of 10 on a time scale of several months. This type of variability is common in water masers and a survey of water maser emission towards mainline OH masers in star formation regions by Batchelor et al. (1980) found that about 60 percent of water masers exhibited variability of up to a factor of two over an eight month period, while the remaining 40 percent exhibited more extensive variability. Given that our initial observations where made in varying weather conditions with comparitively poor pointing accuracy it is difficult to accurately quantify the absolute variations. However, because the water masers have multiple spectral components we are able to determine that variability has occurred by examining the relative amplitudes. Water masers associated with low mass stars are typically both weaker and more variable than those associated with high mass stars (Claussen et al. 1996). So we would expect our observations to be more likely to detect masers associated with high-mass star formation, than those associated with less luminous objects. Variability is also a likely explanation as to why two of the masers detected in the survey with the 26-m Mount Pleasant radio telescope were not detected in the final observations made with the ATCA 6-8 months later, particularly if these masers are associated with low-mass stars.

We have compared the positions of the water masers that we detected with GLIMPSE, *IRAS* and *MSX* sources, as well as 1.2-mm dust clumps (Mookerjea et al. 2004), FIR sources (Karnik et al. 2001), ^{13}CO emission (Bains et al. 2006), CS emission (N. Lo, private communication) and other maser species. The relative positional accuracy of each of these datasets differs, some having significantly poorer positional accuracy than our ATCA observations. We consider a water maser to be associated with a GLIMPSE, *IRAS*, *MSX* or FIR source if it is within a radius of 2, 30, 5 or 60 arcseconds respectively. For water maser G 333.29-0.38 we use more relaxed positional constraints as its position is much less accurately known. For this source we consider the water maser to be associated if it is within 5, 90, 40 or 60 arcseconds of a GLIMPSE, *IRAS*, *MSX* or FIR source respectively. We consider a water maser to be associated with a ^{13}CO, CS or 1.2-mm dust continuum clump if its position falls within the radius of the ^{13}CO, CS or 1.2 mm dust clumps. Table 2 summarises these associations.

Of the nine water masers that we detect four are associated with a GLIMPSE point source, three are associated with an *IRAS* source, two are associated with an *MSX*

source, five are associated with a FIR clump (Karnik et al. 2001) and seven are associated with a 1.2-mm dust clump (Mookerjea et al. 2004). All of the water masers detected in this survey either lie within a ^{13}CO clump identified by Bains et al. (2006) or an identifiable emission peak of the ^{13}CO data. In addition all of the water masers, for which CS data of the GMC was available are associated with CS emission peaks covering a comparable velocity range to the masers.

3.1 Individual Sources

G 332.653-0.621: This water maser was discovered by Kaufmann et al. (1976), who observed it to have a peak flux density of 58 Jy at a velocity of -47 km s^{-1} in 1975. Subsequent observations by Batchelor et al. (1980) during 1977 May showed a single maser feature at -44 km s^{-1} and a slightly weaker intensity of 30 Jy. We measured the peak flux density to be 29 Jy at -45 km s^{-1}, similar to the observations made in 1977. No OH or 6.7-GHz methanol masers have been detected associated with this water maser (Caswell, Haynes & Goss 1980; Ellingsen et al. 1996).

This source is offset from the Hii region G 332.663-0.621 identified by Huang et al. (1999) by 35 arcseconds at a position angle of 58° and is situated within the RCW 106 complex. The closest *IRAS* source is *IRAS* 16158-5055 and is located 11 arcseconds away and has colours typical of an ultra-compact Hii region. This maser is separated from the centre of the nearest ^{13}CO clump by 35 arcseconds and is 45 arcseconds from the centre of the 1.2-mm dust emission peak identified by Mookerjea et al. (2004) at position angles of -79° and -83° respectively.

G 332.826-0.549: This maser was discovered by Braz & Scalise (1982) in 1980 April, who reported it to have a peak flux density of 250 Jy at -70.8 km s^{-1}. We found the intensity peak of the maser to be 239 Jy at -59.1 km s^{-1} with emission covering a range of more than a 20 km s^{-1}. While the velocity range over which emission has been observed has remained roughly constant since the maser's discovery, the relative intensities and velocity of the strongest emission have not, for example observations made by Braz & Scalise (1982) in 1981 May showed a peak at -62 km s^{-1} of 198 Jy.

This maser appears to be associated with the *MSX* source G 332.8269-00.5489 which is offset by 5 arcseconds and may be also associated with *IRAS* 16164-5046 which is located 29 arcseconds away, as well as a FIR source (Karnik et al. 2001). The maser is probably associated with a ^{13}CO clump identified by Bains et al. (2006) and a 1.2-mm dust emission peak identified by Mookerjea et al. (2004), which are separated from the maser by 11 arcseconds and 7.73 arcseconds respectively. It is located about 2 arcminutes from the peak of the RCW 106B complex which is centered on 16:20 -50:52 and is offset from the peak of the 22-GHz continuum source detected in our ATCA observations by 2 arcseconds. The maser is separated from the OH maser G 332.826-0.548 (Caswell 1998) by 8 arcseconds (See fourth sub-image of Figure 2).

G 333.060-0.488: This maser exhibits several spectral features over an 18 km s^{-1} velocity range, with the most prominent having a flux density of 64 Jy at -8.7 km s^{-1}. This source was first observed at Mount Pleasant on 8 August 2005 when the feature at -8.7 km s^{-1} was approximately

6.5 Jy and the secondary feature at about 0 km s^{-1} was 3 Jy, implying a variation of a factor of 10 over an 11 month period. The velocity of this maser is comparable to one of the less dominate features of the velocity profile of the GMC observed by (Bains et al. 2006) (See Figure 7). Plotting of the kinematic distance versus velocity by (Bains et al. 2006) suggests that this maser is likely part of a different molecular cloud located along the line of sight at a distance of approximately 1 kpc.

The ATCA observations detected a 22-GHz continuum source offset from the water maser source by about an arcminute (See third sub-image of Figure 2). The water maser source appears to be associated with GLIMPSE point source G 333.0600-00.4888.

G 333.121-0.434: This source was discovered by Caswell et al. (1974) in 1973 June. Subsequent observations made in 1976 August by Batchelor et al. (1980) showed a decline in the -51 km s^{-1} peak, while improved sensitivity uncovered additional spectral features. We observed the current peak intensity to be 161 Jy at -57.7 km s^{-1} with emission covering the velocity range -60 to -46 km s^{-1}. Like many of the water masers presented here, we observe variability of the most prominent feature of a approximately a factor of two over a nine month period.

This source is located within RCW 106A structure and is offset from two OH masers by about 50 arcseconds (Caswell 1998). The 6.7-GHz methanol maser G 333.121-0.434 (Ellingsen 2005) is separated from the water maser by less than an arcsecond and emission is seen over a similar velocity range to the water maser. This maser falls within FIR, ^{13}CO and 1.2-mm dust clumps with angular separations of 59, 40 and 47 arcseconds from the centre of the respective clumps. We detected a 22-GHz continuum source separated from the water maser by approximately 50 arcseconds which may be associated with the two OH masers observed by Caswell (1998) (See second sub-image of Figure 2).

G 333.221-0.402: The peak flux density of this maser has remained approximately constant over the course of our observations, however, initial observations made in 2005 August showed only one spectral feature, while observations with the ATCA on 2006 July detected four additional peaks. While three of these features can be explained by the improved sensitivity offered by the ATCA the remaining secondary peak of approximately 7 Jy should have been detected in initial observations, suggesting this maser exhibits some variability.

This water maser appears to be associated with GLIMPSE point source G 333.2205-00.4024 and is separated from the centre of the nearest ^{13}CO clump by 33.16 arcseconds. This source falls within 10 arcseconds of the centre of a 1.2-mm dust clump and 42 arcseconds from the centre of a FIR source detected by Karnik et al. (2001).

G 333.29-0.38: This water maser was discovered 2005 June 26 when it was detected in both polarisations and in adjacent spectra, however, when follow-up observations were made during 2005 September and October the peak flux density of the maser was less than 1 Jy. The earlier observations showed the maser to have a single spectral feature of approximately 7 Jy at -49 km s^{-1}, comparable to the velocity of the Hii region, GAL 333.3-00.4, (Huang et al. 1999) which is situated 17 arcseconds away and has a velocity of -52.1
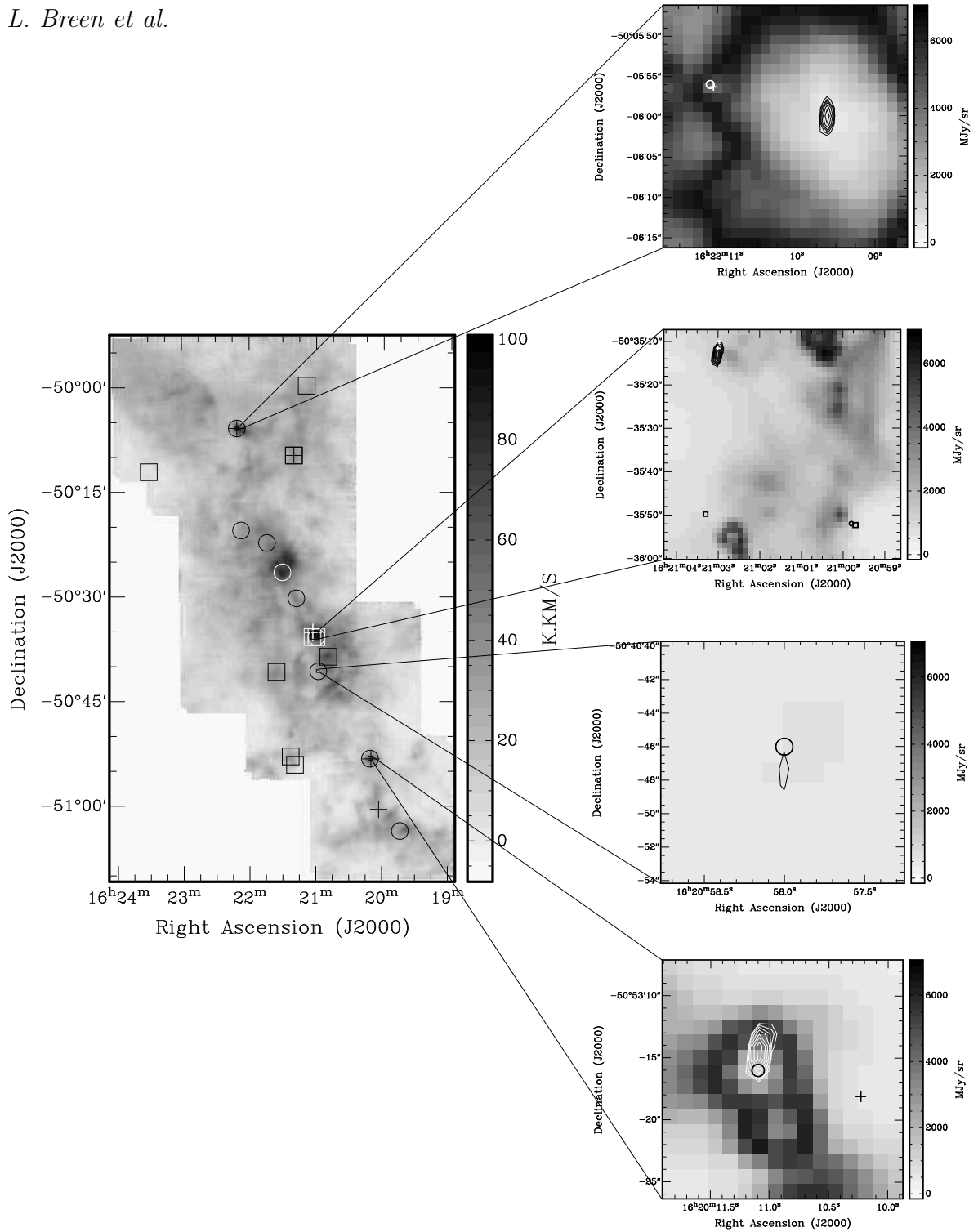
6   *S. L. Breen et al.*

Figure 2. The main image shows the integrated ^{13}CO emission observed by Bains et al. (2006) with the positions of water (circle), methanol (square) and OH (cross) masers overlaid (note that the most central OH maser in the main image is infact two OH sources close together as shown in the second sub-image). The positions of the methanol and OH masers have also been obtained from ATCA observations and have a similar positional accuracy to the water maser positions (Caswell 1998; Ellingsen 2005). In the main image, the size of the shapes is much larger than the positional accuracy, however, the four sub-images (of water masers 9, 4, 3 and 2 respectively) show the positions of the maser species and indicate the positional accuracy of these masers overlayed on a 8.0-μm GLIMPSE image of the region. Also overlaid on the sub-images are the 22-GHz continuum contours detected in our ATCA observation. The first contour in each case is at the 5σ level for the continuum image and they increase in factors of $\sqrt{2}$. Details of the continuum sources can be found in Table 3.

Table 1. 22-GHz water masers detected within the survey regions. Column 1 gives the water maser source number (which is used in later tables), column 9 indicates whether or not each maser was detected in the ATCA observation and column 10 gives the water maser references. ATCA positions are quoted for all water masers with the exeption of G 333.29-0.38 (source number 6). References: * = new source; 1 = Caswell et al. (1974); 2 = Kaufmann et al. (1976); 3 = Braz & Scalise (1982) 4 = Johnston et al. (1972).

Source number	Water maser (l, b)	Right Ascension (J2000)	Declination (J2000)	Peak Flux (Jy)	Peak Vel. wrt LSR (km s^{-1})	Velocity Range (km s^{-1})	epoch	ATCA detection?	Ref
1	G 332.653-0.621	16:19:43.569	-51:03:37.06	28.9	-45.3	-59,-43	2006 July	yes	2
2	G 332.826-0.549	16:20:11.089	-50:53:16.07	239.4	-59.1	-69,-45	2006 July	yes	3
3	G 333.060-0.488	16:20:58.002	-50:40:46.32	64.3	-8.7	-13,5	2006 July	yes	*
4	G 333.121-0.434	16:20:59.762	-50:35:51.55	161.1	-57.7	-60,-46	2006 July	yes	1
5	G 333.221-0.402	16:21:17.913	-50:30:17.99	9.6	-52.0	-58,-48	2006 July	yes	*
6	G 333.29-0.38	16:21:30.4	-50:26:34	7	-49.0	-51,-47	2005 June	no	*
7	G 333.364-0.358	16:21:44.319	-50:22:21.08	3.2	-52.6	-55,-49	2006 July	yes	*
8	G 333.428-0.380	16:22:07.539	-50:20:34.29	12.4	4.1	-6,6	2006 July	yes	*
9	G 333.608-0.215	16:22:11.060	-50:05:55.98	103.3	-49.2	-64,-38	2006 July	yes	4
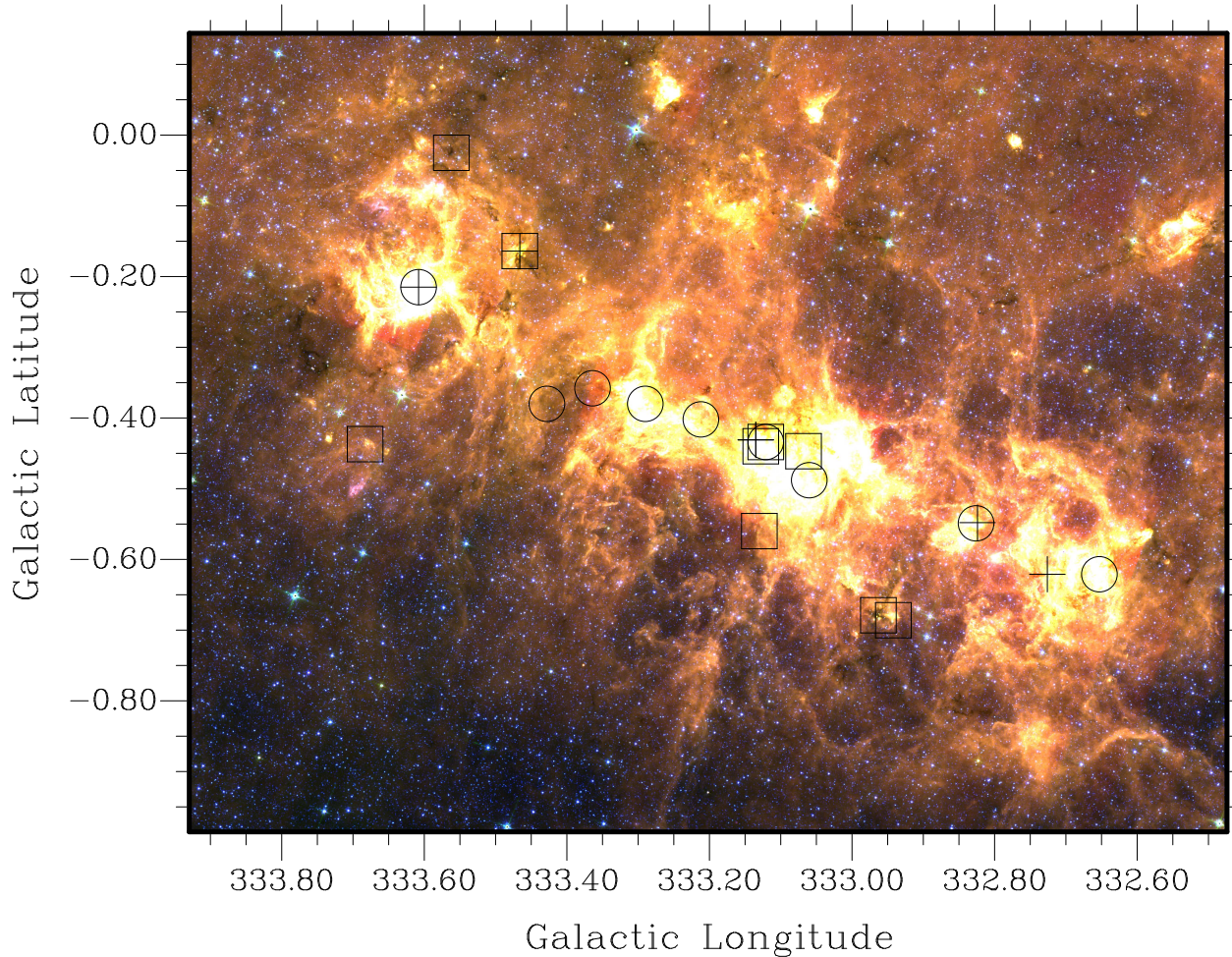
Figure 3. Three colour GLIMPSE image of the GMC where red=8.0-μm green=5.8-μm and blue=3.6-μm. The positions of the nine water masers detected in this survey are represented by circles, positions of the methanol masers observed by Ellingsen (2005) are represented by squares and the positions of the OH masers observed by Caswell (1998) are represented by crosses. Water maser sources 1-9 are numbered in order of increasing longitude.

km s^{-1}. This maser was not detected in the observations made with the ATCA and so we expect that the pointing accuracy is of the order of 1 arcminute. The source is separated from *MSX* source G 333.2898-00.3898 by 33 arcseconds and given the positional accuracy of the maser source may be associated.

G 333.364-0.358: A decline in the peak flux density has been observed since this maser was discovered on 2005 August 25. In the initial observations a peak flux density of 9 Jy was observed compared to the final observations made with the ATCA where a peak flux of 3.2 Jy was recorded. This source is separated from the centre of the nearest ^{13}CO clump by 47.42 arcseconds and the centre of a FIR source detected by Karnik et al. (2001) by 37 arcseconds.

G 333.428-0.380: This maser consists of two main spectral features at velocities of -4.5 and 4.1 km s^{-1} with flux densities of 4 Jy and 12.4 Jy respectively. A decrease in the flux density of the primary feature has been observed since observations made during 2005 April when it had a peak flux density of 26 Jy. This is the only maser detected in our survey for which there is no *IRAS*, *MSX*, 1.2-mm dust or other maser species within 2 arcminutes. There is however a near by ^{13}CO emission peak located at about 40 arseconds from the maser. Like water maser G 333.060-0.488, the velocity of this maser indicates that it is probably part of another molecular cloud located at a distance of approximately 1 kpc Bains et al. (2006).

G 333.608-0.215: This is one of the earliest discovered water masers and was first detected by Johnston et al. (1972) who observed it to have a primary feature at -49 km s^{-1} and a secondary feature at -57 km s^{-1}. Observations in 1976 August by Batchelor et al. (1980) found a 100 Jy peak at -52 km s^{-1}. We detected emission over a 26 km s^{-1} velocity range with the most intense feature of 103 Jy at -49.2 km s^{-1} and a decline in the -52 km s^{-1} feature to about 38 Jy. There is an associated OH maser observed by Caswell (1998) which is displaced from the water maser by less than an arcsecond and shows emission over a velocity range of -48 km s^{-1} to -36km s^{-1}(See first sub-image of Figure 2). This maser is associated with the well known H II region G 333.6-0.2 which is almost totally obscured at optical wavelengths but is one of the brightest objects at longer wavelengths. This maser is probably associated with an *IRAS* source, FIR source, ^{13}CO clump, CS emission and 1.2-mm dust clump.

3.2 22-GHz Continuum Sources

Four radio continuum sources were detected in the ATCA observations. Their properties are summarised in Table 3 and are shown in Figure 6 as well as in the sub-images of Figure 2. Continuum sources which are located away from the centre of the primary beam have had their flux densities corrected to account for beam attenuation.

G 333.826-0.549 This is the strongest radio continuum source detect in our ATCA observations and its peak is located within 2 arcseconds of the water maser G 332.826-0.549. The nearest infrared source is *IRAS* 16164-5046, with which it is possibly associated.

G 333.060-0.489 This is the weakest continuum source that we detected. The source is spatially coincident with GLIMPSE point source G 333.0600-00.4888 as well as the water maser G 333.060-0.488.

G 333.135-0.432 This continuum source while not associated with any water masers, does appear to be associated with two OH masers observed by Caswell (1998) (shown in Figure 2). There is no associated infrared source.

G 333.605-0.212 This continuum source is coincident with the *MSX* source G 333.6046-00.2124 and *IRAS* source *IRAS*16183-4958, both of these sources are separated from the peak of the continuum emission to within 1.3 and 5.8 arcseconds. This source is offset from the nearest water maser that we observe by about 15 arcseconds.

4 DISCUSSION

4.1 Association with Infrared Sources

Ellingsen (2006) found that approximately two-thirds of 6.7-GHz methanol masers have an associated GLIMPSE point source, and less than 10 percent of sources are not associated with mid-infrared emission (at the sensitivity of the GLIMPSE observations). A search of the GLIMPSE catalogue reveals four of the water maser sources detected (all of them new discoveries) have an associated GLIMPSE point source within 2 arcseconds. The details of these GLIMPSE point sources are summarized in Table 4. Of the remaining 5 water masers, the four previously detected sources are all clearly projected against regions of bright mid-infrared emission (see Fig. 3). Ellingsen (2006) suggested that a search for 6.7-GHz methanol masers towards GLIMPSE point sources meeting the criteria [3.6]-[4.5] > 1.3 mag and 8.0 μm magnitude < 10 would detect more than 80 percent of this class of maser. From Table 4 it can be seen that three of the four GLIMPSE point sources associated with water masers satisfy these criteria. Comparing the [3.6]-[4.5] colour of the GLIMPSE sources associated with water masers to those associated with 6.7-GHz methanol masers (see Fig. 16 of Ellingsen), the water masers cluster at the low end of the range observed in the methanol associated sources. The idea that different maser species may trace different phases of the high-mass evolutionary sequence is not new, however, it has been receiving renewed attention lately with as sensitive, high-resolution observations at submillimeter through mid-infrared wavelengths become more readily available. Ellingsen (2006) looked at this question in some detail and we will not repeat the arguments here, however, the striking difference between the relative location of the water and methanol masers in the G 333.2-0.6 GMC, and the less red colours of the water maser associated GLIMPSE sources supports the hypothesis that 6.7-GHz methanol masers may trace a generally earlier evolutionary phase than water masers. The very small water maser sample size prevents us from drawing any firm conclusions, however, it suggests that comparison of the properties of GLIMPSE sources associated with water and methanol masers may provide useful insights relating to this question.

The top and bottom inset images in Fig. 3 each show a ring of diffuse 8.0-μm emission surrounding a darker region. We have closely examined the GLIMPSE images of these regions and believe that this is not due to an instrumental artifact (such as saturation). For the northern most region (associated with the maser G 333.608-0.215) each of the four GLIMPSE wavebands shows a ring like structure and the ra-
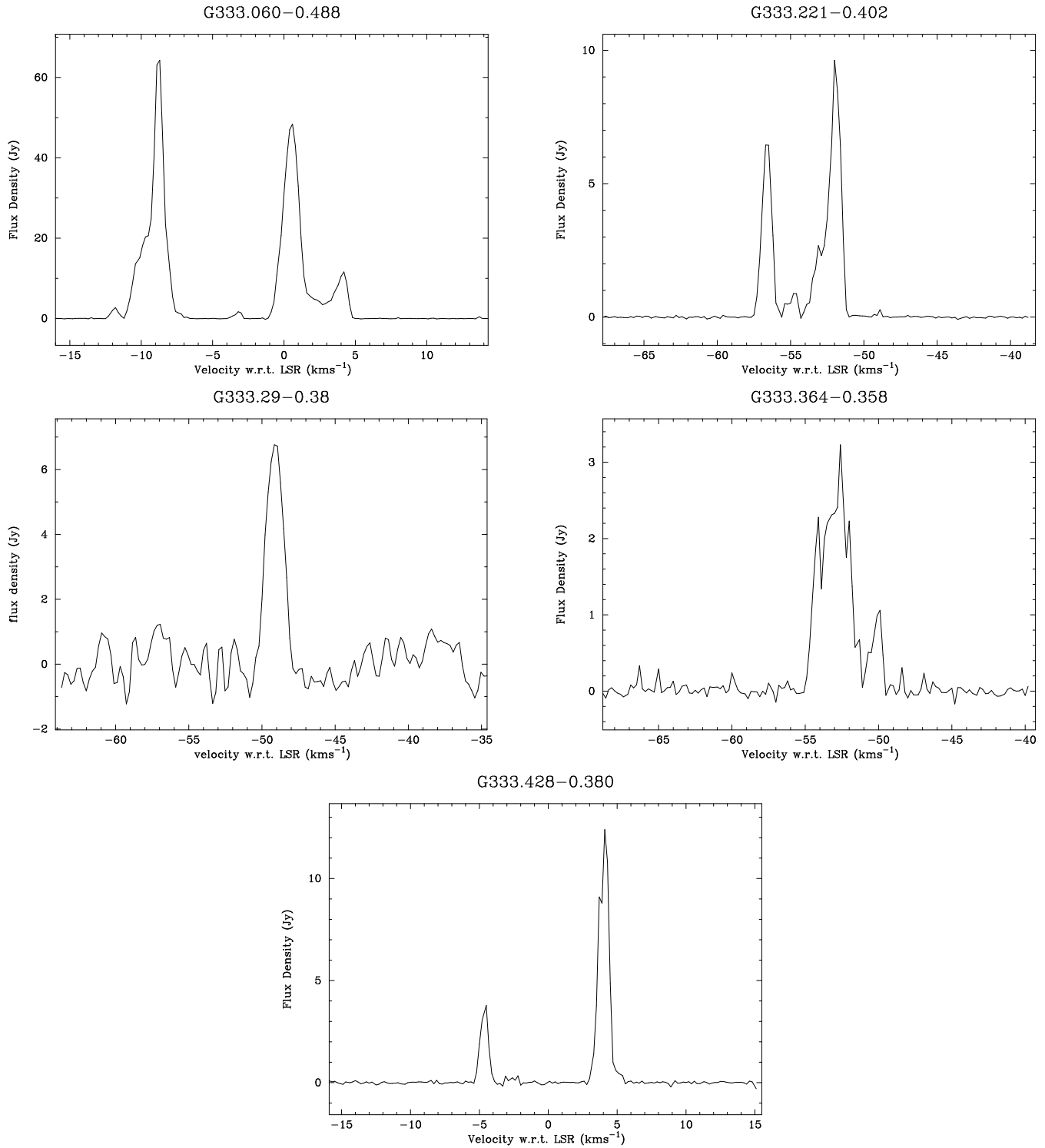
Figure 4. Spectra of the 22-GHz water maser sources discovered in this survey. All of the spectra presented are from the ATCA observations with the exception of 333.29-0.38 which is from the Mount Pleasant observations.

dius of these increases with increasing wavelength. The water maser is embedded within the ring of 8.0-μm emission, but at a unique location within it where the emission at 4.5- and 5.8-μm dominates. For the southern most region (associated with the maser G 332.826-0.549) a ring like structure is seen at 4.5- and 8.0-μm, but at 3.6- and 5.8-μm the emission

fills in the ring. In this case the water maser is located near the centre of the ring. The presence of 22-GHz radio continuum emission at the centre of each of these regions and a general progression to longer wavelength emission with increasing radius is suggestive of internal heating. The dark central regions may be caused either by optical depth ef-
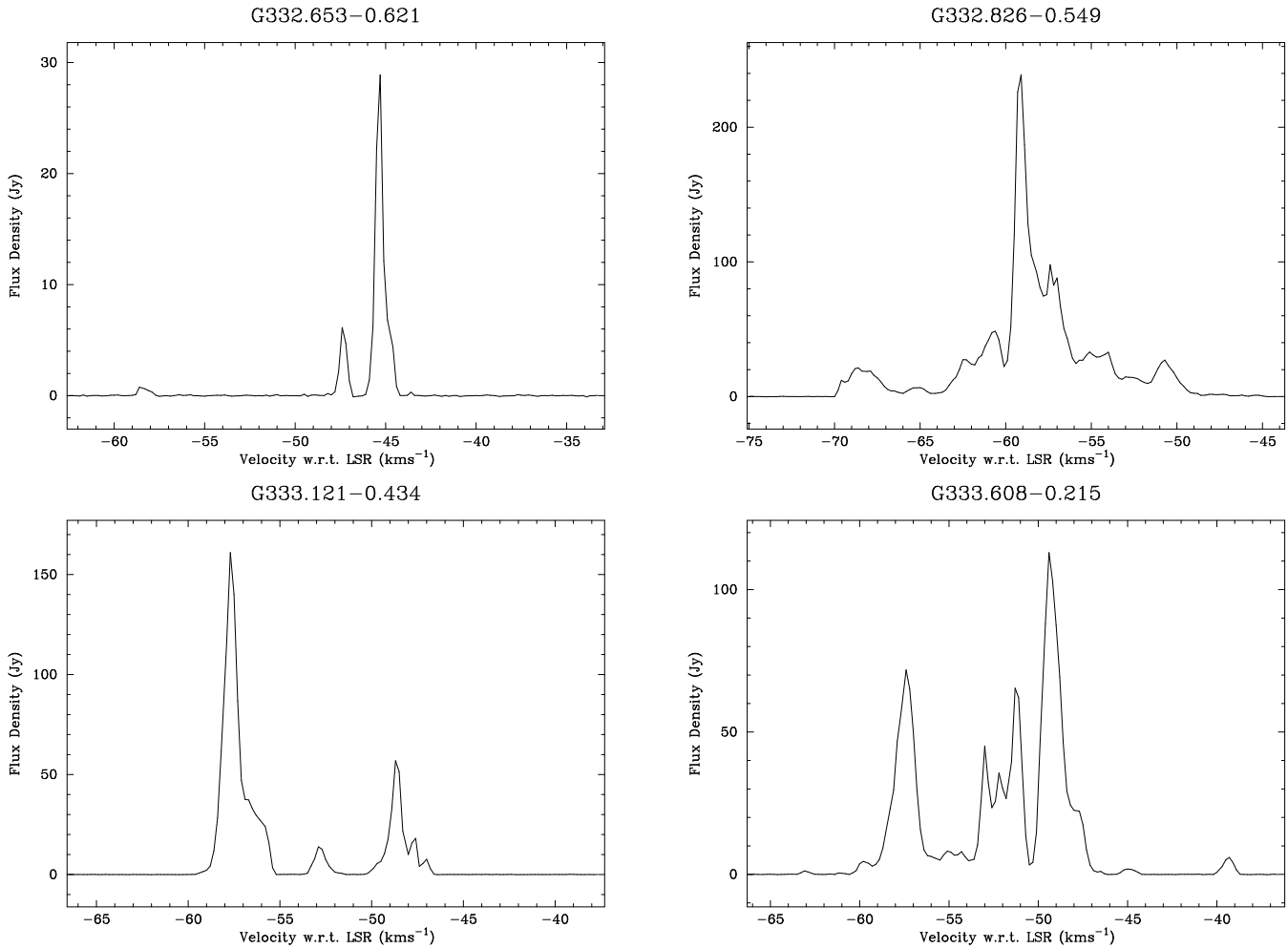
10   *S. L. Breen et al.*

Figure 5. ATCA spectra of the 22-GHz water maser sources detected in the search that have been previously discovered.

Table 2. Summary of all possible associations. Details of GLIMPSE, *IRAS*, *MSX*, FIR, 1.2-mm dust, ^{13}CO and CS sources can be seen in Tables 4, 5, 6, 10, 7 and 9. * indicates the ^{13}CO emission peaks that we identify that were outside the velocity range of clump analysis carried out by Bains et al. (2006). - indicates that no data over a similar velocity to the respective water masers was available.

Source number	GLIMPSE	*MSX*	*IRAS*	FIR	1.2 mm dust	^{13}CO	CS	Methanol maser	OH maser
1	n	n	y	n	y	y	y	n	n
2	y	y	y	y	y	y	y	n	y
3	n	n	n	n	y	y*	-	n	n
4	y	n	n	y	y	y	y	y	n
5	n	n	n	y	y	y	y	n	n
6	y	y	n	y	y	y	y	n	n
7	y	n	n	n	n	y	y	n	n
8	n	n	n	n	n	y*	-	n	n
9	n	n	y	y	y	y	y	n	y

fects, or perhaps through distruction or sweeping out of the dust by a high-mass star. Neither of these explanations is entirely satisfactory though as in the former case we would expect longer wavelength emission to be visible at smaller radii rather than shorter, while in the latter case we would expect to see infrared emission from the central star (which we may in G 332.826-0.549, but don't in G 333.608-0.215). In either scenario further observations of these sources at radio and infrared wavelength are warrented to better understand their nature.

Three of the nine water masers detected in this survey (all previously known sources) have an *IRAS* source within 30 arcseconds of them. Two of the water masers that we

Table 3. 22-GHz continuum sources. Column 1 is the source number of the nearest water maser, Columns 2-4 give the position of the continuum source, column 5 gives the peak of the continuum source in mJy/beam, column 6 gives the total flux density of the continuum source in mJy and column 7 gives the angular separation between the continuum source and the nearest water maser source.

Source number	Continuum Source (l, b)	Right Ascension (J2000)	Declination (J2000)	F_{Peak} (mJy/beam)	Total Flux Density (mJy)	Separation from maser (arcsec)
2	G 332.826-0.549	16:20:11.089	-50:53:14.07	948	1180	2
3	G 333.060-0.489	16:20:58.002	-50:40:47.32	91	126	1
4	G 333.135-0.432	16:21:03.017	-50:35:12.54	720	901	50
9	G 333.605-0.212	16:22:09.605	-50:05:59.98	569	631	15

Table 4. Water masers with GLIMPSE point source associations, here IRAC bands 1, 2, 3 and 4 correspond to 3.6-μm, 4.5-μm, 5.8-μm and 8.0-μm. Column 1 gives the water maser source number (see Table 1 for details), column 2 is the associated GLIMPSE point source, column 3 gives the angular separation between the GLIMPSE point source and the water maser source and colums 4 to 7 show the magnitudes of IRAC bands 1, 2, 3 and 4 for each of the GLIMPSE point sources, while column 8 gives the [3.6]-[4.5] colour for each.

Source number	GLIMPSE point source (l, b)	Separation (arcsec)	IRAC band 1	Magnitude IRAC band 2	(mag) IRAC band 3	IRAC band 4	[3.6]-[4.5] colour (mag)
3	G 333.0600-00.4888	1.3	11.964	10.633	9.258	-	1.331
5	G 333.2205-00.4024	1.8	8.973	7.434	6.368	5.895	1.539
6	G 333.3639-00.3574	0.8	11.263	9.780	8.560	7.551	1.483
7	G 333.4285-00.3809	2.0	14.233	13.373	-	-	0.860

Table 5. Possible infrared and water maser source associations. Column 1 gives the water maser source number (see Table 1 for details), column 2 shows the closest *IRAS* source within 2 arcminutes of the water masers, column 3 gives the angular separation between the water maser sources and the *IRAS* source, column 4 is the closest *MSX* source to within 1 arcminute and column 5 gives the angular separation between the *MSX* source and water maser source.

Source number	*IRAS* source	Separation (arcsec)	*MSX* source	Separation (arcsec)
1	16158-5055	11		
2	16164-5046	29	G332.8269-00.5489	5
6	-		G333.2898-00.3898	33
9	16183-4958	20		

Table 6. Separation from FIR sources, detection at 150 and 210 μm. Positions given are of the peak of the 210 μm (Karnik et al. 2001). Columns are as follows; 1 is the maser source number, 2 is the FIR source number quoted by Karnik et al. (2001), 3 and 4 are the Right Ascension and Declination of the clumps, 5 gives the angular separation between the water maser and the peak of the FIR source, columns 6 and 7 give the FIR source's peak flux densities at 150 and 210 μm respectively and column 8 gives the source luminosity.

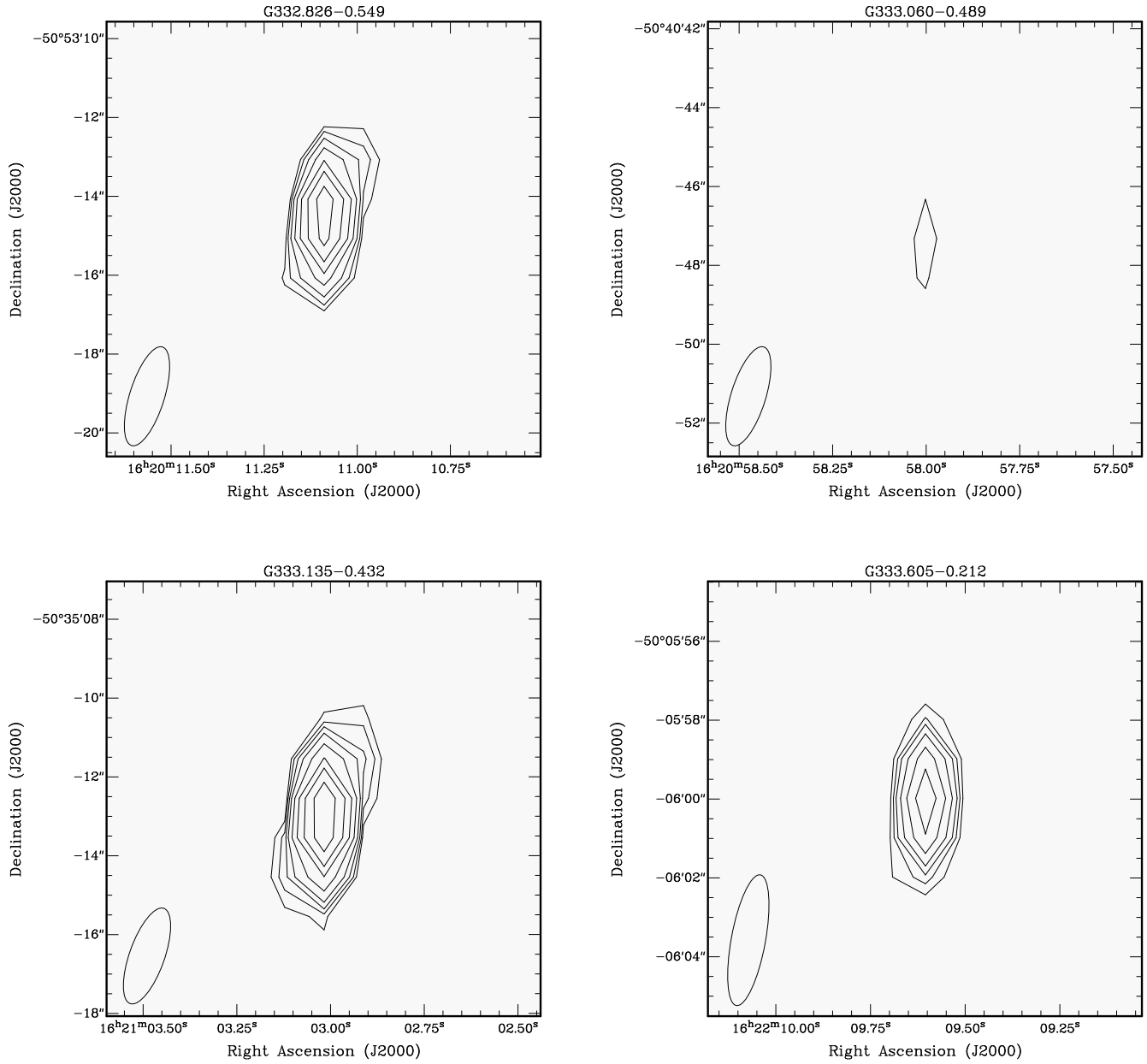| Source number	FIR source number	Right Ascension (J2000)	Declination (J2000)	Separation (arcsec)	150 μm Flux Density (Jy)	210 μm Flux Density (Jy)	Luminosity (10^3 L$_\odot$)
2	S11	16:20:06.0	-50:53:19	48	15380	7790	411
4	S15	16:20:57.9	-50:34:55	59	20811	10009	482
5	S18	16:21:20.3	-50:29:43	42	2180	1043	115
6	S20	16:21:29.8	-50:25:57	37	15572	8015	460
9	S23	16:22:08.9	-50:05:28	35	27841	11555	921

12   *S. L. Breen et al.*

Figure 6. 22-GHz continuum sources, first contour in each case is at the 5σ detection level and increase in factors of $\sqrt{2}$. The peak of each continuum source are 948, 91, 720 and 510 mJy/beam for G 332.826-0.549, G 333.060-0.489, G 333.135-0.432 and G 333.605-0.212. The lowest contour levels are 95, 70, 47 and 70 mJy/beam for G 332.826-0.549, G 333.060-0.489, G 333.135-0.432 and G 333.605-0.212.

observe have an associated *MSX* source. The details of these *IRAS* and *MSX* sources are presented in Table 5.

Karnik et al. (2001) detected 23 FIR sources in a survey of the GMC at 150 and 210 μm. Of the six most luminous of these sources, five have associated water masers.

4.2 Association with Molecular Gas and Dust Clumps

4.2.1 ^{13}CO Clump Associations

Of the nine water masers detected in this survey seven fall within a ^{13}CO clump identified by Bains et al. (2006). Bains et al. (2006) produced *CLUMPFIND* fits of the GMC using the 2D ^{13}CO data integrated over the velocity range -65 km s^{-1} to -35 km s^{-1} which covers the most prominent feature seen in Figure 7. These seven water masers have velocity ranges that fall within that analysed with the
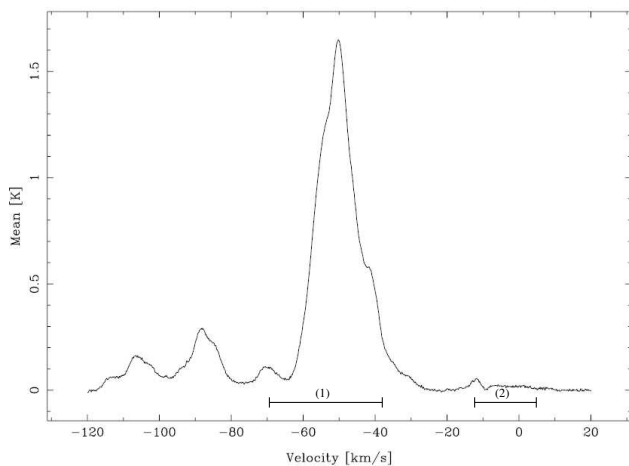
Figure 7. The mean velocity profile of the ^{13}CO emission averaged over the entire field of observations from Bains et al. (2006). Overlaid are the velocity ranges of the water masers. (1) indicates the total velocity range of the seven water masers with comparable velocity ranges; maser sources 1, 2, 4, 5, 6, 7 and 9, while (2) indicates the velocity ranges of maser sources 3 and 8.

$CLUMPFIND$ algorithm, while the remaining two have velocities which fall outside of this range.

We obtained the ^{13}CO data of Bains et al. (2006) in the velocity range -120 km s^{-1} to 20 km s^{-1} which has allowed us to identify additional ^{13}CO emission peaks (or possible clumps) which may be associated with the two masers not coincident with a clump identified by Bains et al. (2006), G 333.060-0.488 and G 333.428-0.380. These emission peaks, like their associated water masers, have velocity ranges which fall outside that analysed by Bains et al.. Water masers G 333.060-0.488 and G 333.428-0.380 show emission over a comparable velocity range of a smaller feature seen in the ^{13}CO emission (Fig. 7).

Details of the ^{13}CO clumps identified by Bains et al. (2006) and the ^{13}CO emission peaks that we identify along with their associated water maser sources are summarized in Table 7, while clump properties identified by Bains et al. (2006) are presented in Table 8. The velocity ranges of the ^{13}CO clumps or emission peaks have been obtained from visual inspection of the data and have more extensive velocity ranges than the associate water maser emission in all cases with the exception of water masers G 333.060-0.488 and G 333.428-0.380. Interestingly these two water masers have similar velocity ranges which are offset from the velocity range of the most prominent feature shown in the velocity profile of the GMC. In the majority of cases the velocity of the peak flux density of the water masers are within a few km s^{-1} of the velocity of the associated peak ^{13}CO emission.

4.2.2 CS Emission Associations

The GMC has been mapped in CS emission by the Delta Quadrant Survey Team as part of the ongoing project at University of New South Wales. CS emission is sensitive to higher densities and as a result the mapped region is less extensive than that covered in the ^{13}CO mapping (and has been obtained in advance of publication as a result of correspondence with Nadia Lo from UNSW). Thich means that

CS data was not available for two of the positions of the detected water masers. We inspected the data over a velocity range of -80 km s^{-1} to -20 km s^{-1} and identified CS emission peaks near all of the seven water masers for which CS data was available. The details of these emission peaks and their associated water masers are summarized in Table 9.

Unlike the ^{13}CO emission, CS emission is observed over a smaller velocity range than the associated water maser emission, however like the ^{13}CO emission the velocity of the peak flux density of the water masers correlates to within a few km s^{-1} with the velocity of the CS emission peaks. The association of the water masers with CS emission indicates that the water masers are probably associated with massive star formation and not their low mass counterparts.

4.2.3 Association with 1.2-mm Dust Emission Peaks

Seven of the water masers that we detect are associated with a 1.2-mm dust emission peak observed by Mookerjea et al. (2004) and the properties of the dust clumps are summarized in Table 10. Mookerjea et al. (2004) identified 95 1.2-mm dust clumps within the GMC and 73 of these fall within our observed regions. A statistical analysis of the 1.2-mm clumps that fall within the observed regions is presented in Section 4.3.

4.3 ^{13}CO and 1.2-mm Dust Clump Analysis

In order to investigate the properties of the molecular gas and dust in the regions with associated water maser emission we have fitted a Binomial generalized linear model (GLM) (McCullagh & Nelder 1989) to the maser presence/absence data using ^{13}CO and 1.2-mm dust clump properties reported by Bains et al. (2006) and Mookerjea et al. (2004) respectively, as predictors. In the case of the ^{13}CO clumps the properties considered were peak ^{13}CO brightness (10 K km s^{-1}), ^{13}CO brightness summed over all the pixels in the clump (10 K km s^{-1}), clump radius (pc), ^{13}CO column density (10^{16} cm^{-2}) and the total LTE molecular mass calculated from the ^{13}CO data. In the case of the 1.2-mm dust clump analysis the properties F_{peak} (mJy/beam), radius (pc), F_v (Jy), mass (M$_\odot$) and n_{H_2} (10^4 cm^{-3}) where investigated as predictors. A Binomial GLM predicts the probability p_i of finding a maser in the ith clump, in terms of the clump properties x_{1i} x_{2i} $x_{3i} \ldots x_{mi}$. The model takes the form

$$y_i \quad \sim \quad \text{Bin}(1, p_i)$$
$$\log\frac{p_i}{1-p_i} \quad = \quad \beta_0 + \beta_1 x_{1i} + \beta_2 x_{2i} + \ldots + \beta_m x_{mi}$$

where y_i is the maser presence or absence in the ith clump and β_0, β_1, $\beta_2 \ldots \beta_m$ are the regression coefficients to be estimated.

To test the significance of individual clump properties all possible single term models were fitted, and compared by analysis of deviance to the null model consisting of only an intercept. Stepwise model selection based on the Akaike Information Criteria (AIC) (Burnham & Anderson 2002) was used to select the most parsimonious model with the greatest predictive power. The AIC is a trade off between goodness of fit and model complexity and is defined as

14   *S. L. Breen et al.*

Table 7. Water maser sources with nearby ^{13}CO clumps identified by Bains et al. (2006) or emission peaks as identified by visual inspection of the data used by Bains et al. (2006). Column 1 is the water maser source number (see Table 1 for details), column 2 and 3 give the velocity range and the velocity of the peak emission of the water maser, column 4 gives the ^{13}CO clump number from Bains et al. (2006) if applicable, columns 5 and 6 show the right ascension and declination of the ^{13}CO clump or alternatively the ^{13}CO emission we identified from the ^{13}CO data from Bains et al. (2006), columns 7 and 8 give the velocity range and the velocity of the ^{13}CO emission peak as we have identified and column 9 is the separation between the centre of the clump that Bains et al. (2006) reported or the emission peak that we identified.

Source number	Velocity Range (km s^{-1})	Peak Velocity (km s^{-1})	^{13}CO source number	Right Ascension (J2000)	Declination (J2000)	Velocity Range (kms^{-1})	Peak Velocity (kms^{-1})	Separation (arcsec)
1	-59,-43	-45.3	9	16:19:40	-51:03:27	-60,-43	-50	35
2	-69,-45	-59.1	7	16:20:11	-50:53:27	-65,-44	-55	11
3	-13,5	-8.7	-	16:20:58	-50:40:39	-9,-2	-6	8
4	-60,-46	-57.7	1	16:21:03	-50:35:27	-64,-45	-51	40
5	-58,-48	-52.0	14	16:21:21	-50:30:03	-57,-40	-52	33
6	-58,-47	-49.0	2	16:21:31	-50:26:51	-58,-45	-52	23
7	-55,-49	-52.6	22	16:21:42	-50:21:39	-67,-42	-51	48
8	-6,6	4.1	-	16:22:05	-50:21:02	-1,10	6	40
9	-64,-38	-49.2	5	16:22:08	-50:06:27	-61,-32	-46	42

Table 8. Properties of the ^{13}CO clumps (Bains et al. 2006). Column 1 is the number of the associated water maser source, column 2 is the ^{13}CO clump number (Bains et al. 2006), column 3 is the peak ^{13}CO brightness, column 4 is the ^{13}CO brightness summed over all the pixels in clump, column 5 is the clump radius, column 6 is the ^{13}CO column density and column 7 is the total LTE molecular mass.

Source number	^{13}CO Clump	Peak (10 K km s^{-1})	Sum (10^3 K km s^{-1})	Radius (pc)	N(^{13}CO) (10^{16} cm^{-2})	Mass (10^3 M$_\odot$)
1	9	10.5	13.3	1.7	6.6	4.6
2	7	12.0	14.4	1.8	6.2	5.0
4	1	18.5	46.0	2.6	10.1	16.0
5	14	8.8	15.7	1.8	6.9	5.5
6	2	15.8	41.4	2.4	10.3	14.4
7	22	8.9	25.0	2.2	7.6	8.7
9	5	13.8	27.4	2.2	7.9	9.5

$$AIC = -2(\text{max log likelihood}) + 2(\text{number of parameters})$$

with the preferred model being the model with the lowest AIC (Venables & Ripley 2002).

For ease of comparison between the data sets box plots were created for each of the clump propertiesg. The solid horizontal line in each of these plots represents the median of the data. The box represents the 25th to the 75th percentile, while the vertical line from the top of the box represents data from the 75th percentile to the maximum value and the vertical line form the bottom of the box represents data from the 25th percentile to the minimum value. Outliers are represented by dots. Box plots of each of the clump properties of both the ^{13}CO clumps and the 1.2-mm dust clumps are shown in Figures 8 and 9 respectively.

4.3.1 ^{13}CO Clump Results

Fits of the single term addition Binomial model to the ^{13}CO clump properties reported by Bains et al. (2006), showed an increasing probability of the presence of a maser was associated with all of the tested factors (peak ^{13}CO brightness, ^{13}CO brightness summed over all the pixels in the

clump, clump radius, ^{13}CO column density and the total LTE molecular mass calculated from the ^{13}CO data). This means that any of the clump properties (in isolation) gives an indication of the likelihood of maser presence. Table 11 gives a summary of the single term addition Binomial model. The same information is shown graphically in Figure 8 which clearly illustrates that for all clump properties there is a difference between the ^{13}CO clumps that have an associated water maser and those that do not. In general the ^{13}CO clumps with associated water masers are bigger, denser and brighter. The most parsimonious model for predicting maser presence involved the peak ^{13}CO brightness, clump radius and the total LTE molecular mass calculated from the ^{13}CO data. This means that if the peak ^{13}CO brightness, radius and mass is known for a ^{13}CO clump then a probability of maser presence can be determined. The estimated regression relation is

$$\log \frac{p_i}{1 - p_i} = -21.2018 + 1.3037 x_{peak} + 8.0589 x_{radius}$$
$$-1.2290 x_{mass},$$

Table 9. Water masers sources with nearby CS emission peaks. Column 1 is the water maser source number, columns 2 and 3 give the velocity range and velocity of emission peak, columns 4 and 5 are the right ascension and declination of the CS emission peak, columns 6 and 7 show the velocity range and the emission peak of the CS emission and column 8 shows the angular separation between the water maser source and the CS emission peak.

Source number	Velocity Range (kms^{-1})	Velocity Peak (kms^{-1})	CS Right Ascension (J2000)	Clump Declination (J2000)	Velocity Range (kms^{-1})	Peak Velocity (kms^{-1})	Separation (arcsec)
1	-59,-43	-45.3	16:19:40	-51:03:30	-56,-44	-50	33
2	-69,-45	-59.1	16:20:11	-50:53:19	-61,-51	-55	4
4	-60,-46	-57.7	16:21:03	-50:34:56	-61,-44	-53	63
5	-58,-48	-52.0	16:21:22	-50:30:46	-57,-48	-51	45
6	-58,-47	-49.0	16:21:29	-50:26:31	-58,-45	-51	12
7	-55,-49	-52.6	16:21:41	-50:23:19	-55,-45	-49	69
9	-64,-38	-49.2	16:22:08	-50:06:17	-58,-39	-47	40

Table 10. Maser sources with nearby 1.2-mm dust clumps identified by Mookerjea et al. (2004). Column 1 is the water maser source number, column 2 is the dust clump number, columns 3 and 4 give the right ascension and declination of the dust clump, column 5 is the angular separation between the water maser and associated dust clump, column 6 gives the clump radii, column 7 is the total integrated flux densities of the clumps and column 8 gives the estimated mass of the clumps assuming a temperature of 40 K.

Source number	1.2-mm dust source	Right Ascension (J2000)	Declination (J2000)	Separation (arcsec)	F_{peak} (mJy/beam)	Radius (pc)	F_v (Jy)	Mass $M_\odot$	n_{H_2} 10^4
1	MMS84	16:19:38.9	-51:03:28	45.05	2499	1.48	21.9	2871	2.45
2	MMS68	16:20:11.9	-50:53:17	7.73	12460	1.70	36.1	5548	2.56
3	MMS51	16:20:52.1	-50:40:51	56.29	348	1.11	2.7	1029	0.73
4	MMS39	16:21:03.7	-50:35:23	47.13	8925	1.19	32.6	4584	6.18
5	MMS33	16:21:18.6	-50:30:25	9.60	1095	0.90	3.5	1325	1.76
6	MMS29	16:21:32.7	-50:27:12	43.89	6502	1.27	24.7	9281	4.38
9	MMS5	16:22:10.1	-50:06:06	13.63	40013	1.88	129.5	15936	5.44

Table 11. Analysis of deviance table for the single term models, showing the AIC and the deviance together with the associated likelihood ratio statistic and p-value for the test of the hypothesis that the satted single term model provides no better fit than the null model consisting only of an intercept.

Predictor	AIC	Deviance	LRT	p-value
none	39.098	37.098		
Peak	28.774	24.774	12.325	0.000447
Sum	35.227	31.227	5.871	0.015394
Radius	34.063	30.063	7.035	0.007994
Density	34.615	30.615	6.483	0.010892
Mass	35.265	31.265	5.833	0.015729

where x_{peak}, x_{radius} and x_{mass} represent clump properties peak ^{13}CO brightness (10 Kkm s^{-1}), radius (pc) and mass (10^3 M$_\odot$). The full regression summary is shown in Table 12.

Setting the threshold probability of the ^{13}CO clump model at 0.5 (i.e. a value greater than 0.5 suggests a water maser will be associated with a clump, while a value less suggests no water maser), we find the misclassification rates to be low. Of the 40 ^{13}CO clumps that fall in our observation regions which correspond the the main part of the GMC (-65 km s$^{-1} \leq$ v$_{LSR} \leq$ -35 km s^{-1}), seven have an associated water maser while our model predicts that five of these have

Table 12. Summary table for the Binomial regression model, showing for each predictor the estimated coefficient and its standard error, and the standardised z-value and p-value for the test of the hypothesis that $\beta_i=0$.

Predictor	Estimate	Std. Error	z value	p-value
Intercept	-21.2018	9.0538	-2.342	0.0192
Peak	1.3037	0.5041	2.586	0.0097
Radius	8.0589	5.0069	1.610	0.1075
Mass	-1.2290	0.6153	-1.997	0.0458

an associated water maser and returns a false negative for the remaining two clumps. There are 33 clumps within the survey regions that do not have associated water masers, our model predicts that 31 of these do not have associated water masers but returns a false positive for the remaining two clumps.

4.3.2 1.2-mm Dust Clump Results

In terms of the 1.2-mm dust clump properties, fits of the single term addition Binomial model showed an increasing probability of the presence of a maser was associated with increasing value of all of the clump properties reported by (Mookerjea et al. 2004). Table 13 gives a summary of the
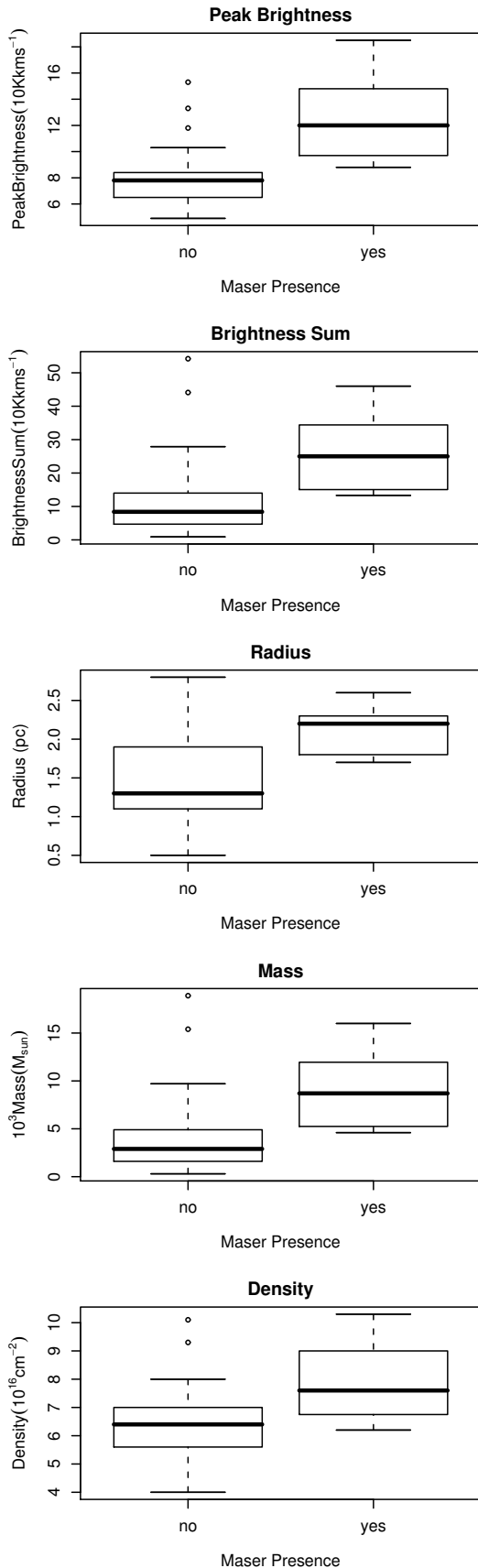
16 *S. L. Breen et al.*

Figure 8. Box plots of each of the ^{13}CO clump properties split into the categories of yes and no, referring to maser presence and absence respectively.

Table 13. Analysis of deviance table for single term models, showing the AIC and the deviance together with the associated likelihood ratio statistic and p-value for the test of the hypothesis that the stated single model provides no better fit than the null model consisting only of an intercept.

Predictor	AIC	Deviance	LRT	p-value
none	46.130	48.130		
$\mathbf{F}_{peak}$	28.088	24.088	22.042	2.668e-06
Radius	24.330	20.330	25.800	3.787e-07
$\mathbf{F}_v$	25.428	21.428	24.702	6.693e-07
Mass	27.467	23.467	22.663	1.930e-06
Density	39.969	35.969	10.160	0.001435

Table 14. Summary table for the Binomial regression model, showing for each predictor the estimated coefficient and the standardised z-value and p-value for the test of the hypothesis that $\beta_i=0$.

Predictor	Estimate	Std. Error	z value	p-value
Intercept	-11.477	3.537	-3.245	0.00118
Radius	9.174	3.163	2.900	0.00373

single term addition. This means that any one of the clump properties may give an indication of the likelihood of maser presence. There is a significant difference in the clumps with associated water masers versus those without, as evident in Figure 9, clumps with associated masers are bigger, denser and have higher flux densities than clumps where we see no associated water maser. The most parsimonious model for predicting maser presence involved only the radius of the 1.2-mm dust clumps. This equation allows the probability of maser presence to be predicted knowing only the radius of a 1.2-mm dust clump. The estimated regression relation is

$$\log \frac{p_i}{1 - p_i} = -11.477 + 9.174 x_{radius},$$

where x_{radius} is the radius of the 1.2-mm dust clump in pc. The regression summary of this model is shown in Table 14.

The misclassification rates for the model, given a probability of 0.5 of maser presence within a given clump are again low in predicting the clumps that have no associated water maser. Of the 73 1.2-mm dust clumps that fall within our survey region, seven have an associated water maser, while 66 do not. Our model predicts that 65 of the 66 clumps with no associated water maser will not have an associated water maser and returns a false-positive result for the remaining clump. The model predicts that of the seven clumps that have an associated water maser only four will have an associated water maser and returns a false negative for the remaining three clumps.

5 CONCLUSIONS

Regions within the GMC associated with RCW 106 have been surveyed for 22-GHz water masers. This resulted in
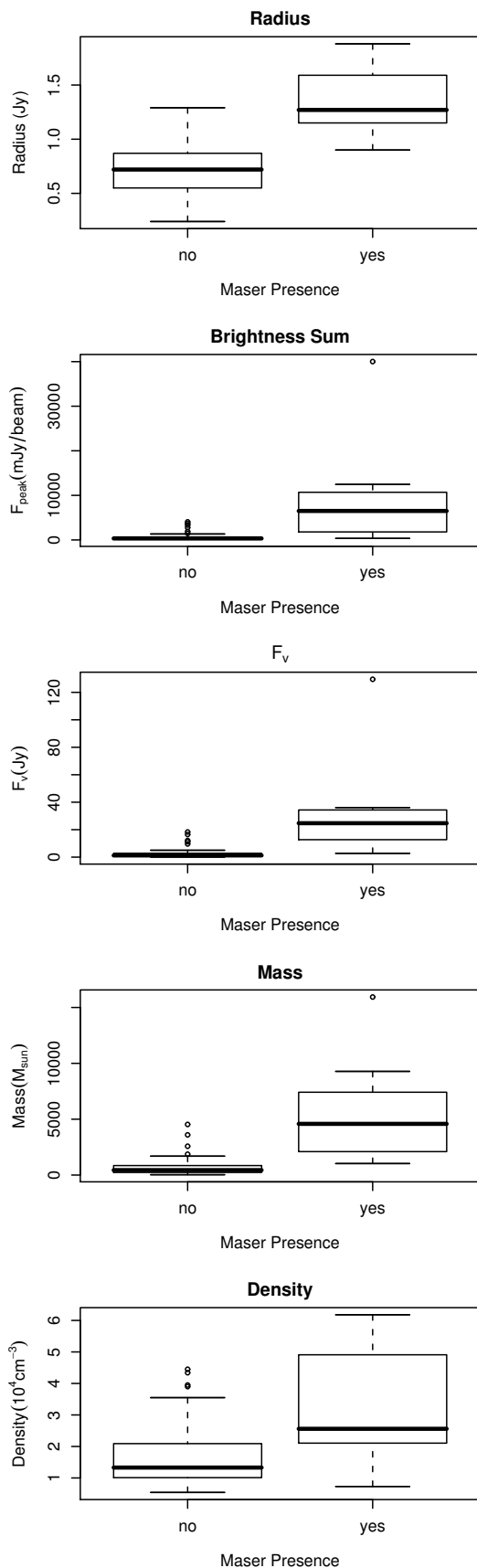
Figure 9. Box plots of the 1.2-mm dust clump properties split into the categories of yes and no, referring to maser presence and absence respectively.

the detection of nine water masers (five of these being new detections) and four 22-GHz continuum sources. All of the water masers that we observed have exhibited some level of variability over the 11 month course of these observations. The most extensive temporal variability was observed in water maser G 333.060-0.488, which showed a variation in peak flux density of a factor of 10 over the observational period. The GMC has previously been searched for 6.7-GHz methanol masers (Ellingsen et al. 1996) and main-line OH masers (Caswell, Haynes & Goss 1980). In addition to the nine water masers detected there are four 6.7-GHz methanol masers (Ellingsen et al. 1996) and three OH masers (Caswell, Haynes & Goss 1980) within the regions surveyed here. All of the three species of masers have sub-arcsecond positional accuracy which allows a comparison of the relative positions of the respective maser species. The water masers that we detect lie along the main axis of star formation within the GMC while the methanol masers are located near the periphery. We find there to be little overlap between the sites of the different maser species, in fact there are only two associations with other maser species. There is one association with a 6.7-GHz maser and one association with an OH maser.

Four of the new water maser detections are associated with a GLIMPSE point source, of similar colour to those associated with detected 6.7-GHz methanol masers. There is a slight bias for the water maser associated sources to be less red. This coupled with the relative positions of the water masers and the 6.7-GHz methanol masers with respect to the main axis of star formation lends support to the hypothesis that 6.7-GHz methanol masers trace an earlier evolutionary phase than water masers.

All of the water masers are associated with a ^{13}CO emission peak that we identify or a clump reported by Bains et al. (2006). Statistical investigation of the ^{13}CO (Bains et al. 2006) and 1.2-mm dust (Mookerjea et al. 2004) clumps shows that there is a strong increase in likelihood of water maser detection with increased clump radius, mass, density and brightness. After fitting a Binomial generalized linear model to the maser presence data using the clump properties of Bains et al. (2006) and Mookerjea et al. (2004) as predictors we obtained the simplest models with the greatest maser predictive power. In the case of the 1.2-mm dust clumps our model uses only clump radius to predict the likelihood of the clump having an associated water maser. However the model generated for ^{13}CO clumps takes into account radius, brightness and mass. These models have a low misclassification rate and may allow more efficient targeted searches for water masers than those previously conducted towards other species of masers or mid-infrared sources. While our survey was of comparatively small scale, we believe that the results are indicative of the likelihood of occurrence of water masers with respect to ^{13}CO and 1.2-mm dust clumps.

18 *S. L. Breen et al.*

REFERENCES

Bains I. et al., 2006, MNRAS, 367, 1609

Batchelor R. A., Caswell J. L., Haynes R. F., Wellington K. J., Goss W. M., Knowles S. H., 1980, Aust. J. Phys., 33, 139

Becklin E. E., Frogel J. A., Neugebauer G., Persson S. E., Wynn-Williams C. G, 1973, ApJ, 182,125

Beuther H., Walsh A., Schilke P., 2002, A&A, 390, 289

Brand J., Cesaroni R., Comoretto G., Felli M., Palagi F., Palla F., Valdettaro R., 2003, A&A 407, 573

Braz M. A., Scalise Jr. E., 1982, A&A., 107, 272

Burnham K. P., Anderson D. R., 2002, "Model Selection and Multimodel Inference, A Practical Information - Theoretic Approach", Second Edition, Springer, New York

Caswell J. L., Batchelor R. A., Haynes R. F., Huchtmeier W. K., 1974, Aust. J. Phys., 27, 417

Caswell J. L., Haynes R. F., Goss W. M., 1980, Aust. J. Phys., 33, 639

Caswell J. L., 1998, MNRAS, 297, 215

Cheung A. C., Rank D. M., Townes C. H., Thornton D. D., Welch W. J., 1969, Nature, 221, 626

Churchwell E., Walmsley C. M., Cesaroni R., 1990, A&AS, 83, 119

Claussen M. J., Wilking B. A., Benson P. J., Wootten A., Myers P. C., Terebey S., 1996, ApJS, 106, 111

Elitzur M., Hollenbach D. J., McKee C. G., 1989, ApJ, 346, 983

Ellingsen S. P., 2005, MNRAS, 359, 1498

Ellingsen S. P., 2006, ApJ, 638, 241

Ellingsen S. P., von Bibra M. L., McCulloch P. M., Norris R. P., Deshpande A. A., Phillips C. J., 1996, MNRAS, 280, 378

Gillespie A. R., Huggins P. J., Sollner T. C. L. G., Phillips T. G., Gardner F. F., Knowles S. H., 1977, A&A, 60,2 21

Hanslow L. A., 1997, Honours Thesis, Univ. Tasmania

Huang M., Bania T. M., Bolatto A., Chamberlin R. A., Ingalls J. G., Jackson J. M., Lane A. P., Stark A. A., Wilson R. W., Wright G. A., 1999, ApJ, 517, 282

Johnston K. L., Robinson B. J., Caswell J. L, Batchelor R. A, 1972, ApL, 10, 93

Karnik A. D., Ghosh S. K., Rengarajan, T. N., Verma R. P., 2001, MNRAS, 326, 293

Kaufmann P., Gammon R. H., Ibanez A. L., Lepine J. R. D., Marques Dos Santos P., Paes de Barros M. H., Scalise E., Schaal R. E., Zisk S. H., Carter J. C., 1976, Nature, 260, 360

Lockman F. J., 1979, ApJ, 232, 761

McCullagh P., Nelder, J. A., 1989, "Generalized linear models", Chapman and Hall, London

Mookerjea B., Kramer C., Nielbock M., Nyman L., 2004, A&A, 426, 119

Pestalozzi M. R., Minier V., Booth R. S., 2005, A&A, 432, 737

Rodgers A. W., Campbell C. T., Whiteoak J. B., 1960, MNRAS, 112, 103

Roman-Lopes A., Abraham Z., Lepine J. R. D., 2003, Astron. J., 126, 1896

Sault R. J., Teuben P. J., Wright M. H., 1995, ASP Conf. Ser. 77, Ed. Shaw, R. A., Payne, H. E., Hayes, J. J. E., 433

Simon, R., Jackson, J. M., Clemens, D. P., Bania, T. M., Heyer, M. H., 2001, ApJ, 551,747

Szymczak M., Kus A. J., Hrynek G., Kepa A., Pazderski E., 2002, A&A, 392, 277

Szymczak M., Pillai T., Menten K. M., 2005, A&A, 434, 613

Torrelles J. M., Patel N. A., Gómez J. F., Anglada G., 2002, in Revista Mexicana de Astronomia y Astrofisica Conference Series, Ed. Henney W. J., Steffen W., Binette L., Raga A., 13, 108

Valdettaro R., Palla F., Brand J., Cesaroni R., Comoretto G., Di Franco S., Felli M., Natale E., Palagi F., Panella D., Tofani G., 2001, A&AS, 368, 845

Venables W. N., Ripley B. D., 2002, "Modern applied statistics with S", Fourth Edition, Springer, New York

Williams J. P., de Geus E. J., Blitz L., 1994, ApJ., 428, 693